Appendix D: Use of Wave Scenarios to Assess Potential Submerged Oil Mat (SOM) Formation Along the Coast of Florida and Alabama

P. Soupy Dalyander, Joseph W. Long, Nathaniel G. Plant, David M. Thompson

Overview

Oil from the Deepwater Horizon spill mixed with sediment in the surf zone to form denser-than-water sediment oil residue of various size, ranging from small (cm-scale, surface residual balls, SRBs) pieces to large mats (100-m scale, surface residue mats, SR mats). Once SR mats formed in the nearshore or in the intertidal zone, they may have become buried by sand moving cross-shore (perpendicular to the beach) or alongshore (parallel to the beach). To assist in locating possible sites of buried oil, wave scenarios previously developed by USGS were used to determine the depths at which surface oil had the potential to mix with suspended sediment. For sediment to mix with floating oil and form an agglomerate of sufficient density to sink to the seafloor, either the water must have been very shallow (e.g., within the swash zone) or sediment must have been suspended to the water surface in sufficient concentrations to create a denser-than-sea water sand/oil agglomerate. The focus this study was to analyze suspended sediment mixing with surface oil in the surf zone beyond the swash zone, in order to define the seaward limit of mat formation. A theoretical investigation of sediment dynamics in the nearshore zone suggested that non-breaking waves do not suspend enough sediment to the surface to form sinking sand/oil agglomerates. We concluded that the possibility for agglomerate formation existed in the surf zone when plunging breakers and/or very high wave-induced turbulence dissipation

occurred when oil was present. The potential locations of submerged oil mats (SOMs) are sites where: (1) possible agglomerate formation occurred; (2) sediment accreted post-oiling and buried the SOM; and, (3) the bathymetry has not subsequently eroded to re-expose any mat that may have formed at that site. This appendix describes our approach for addressing (1) and our methods for evaluating water level variations that might affect (2) and (3).

Objectives

The objectives of this effort were to:

- Identify the probable distribution of water depths where wave breaking occurred across the domain of interest to determine the depths of possible mat formation.
- Combine the analysis of wave breaking depth with imagery-based estimates of bathymetry and morphological features pre- and post-oiling to identify the cross-shore probability of mat formation and the likelihood that buried mats persist at these sites.
- Improve understanding of factors controlling oiled sediment washing onshore and reduce uncertainties in predicting present and future oiled sediment distributions.

Background: Physical Processes

In the swash zone, shallow depths put oil in direct contact with the seafloor/beach surface, allowing the formation of surface oil residue mats. The question addressed in the current study was if conditions deeper in the surf zone were energetic enough to suspend sediment and mix it with oil in sufficient quantities to create an agglomerate dense enough to sink to the seafloor. Using the density of oil (ρ_o = 900 kg/m^3) and quartz sand (ρ_s = 2650 kg/m^3), we determined the volume fraction of sand (f_s) required for the density of resulting agglomerate (ρ_a) to be denser than seawater (1027 kg/m^3) according to

$$\rho_a = f_s \rho_s + (1 - f_s)\rho_o \quad (1)$$

Solving this equation for f_s, the threshold for neutral buoyancy (above which the agglomerate would begin to sink) is 7% sand by volume, which equates to a mass concentration of about 200 kg/m^3 and a mass fraction of nearly 20%. Thus, assuming the concentration of sand in oiled sediment was the same as in the upper water column, the suspended sediment load at the water surface must have been greater than about 200 kg/m^3 for the agglomerate to have started sinking.

These are extremely high concentrations of sediment, and there is little observational or theoretical basis for determining when, or if, these concentrations might occur. The suspended sediment load at the surface under non-breaking waves was calculated for the wave scenarios following methods prescribed in Soulsby (1997) using the Nielson (1992) formulation for sediment concentration and the Grant and Madsen (1982) formulation to determine the presence and characteristics of wave-induced seabed ripples. Even under the most energetic of wave conditions considered, e.g. wave height greater than 2.0 m (Plant et al., 2013), the surface sediment concentration under non-breaking waves in water depths greater than 10 cm was on the order of a magnitude of 1 kg/m^3 or less. Thus, without the turbulence and convective mixing generated by breaking waves, which suspend sediment from the seafloor and simultaneously mix oil downward from the surface, insufficient sediment mixed with oil to form agglomerates.

The most likely conditions for achieving the required suspended sediment concentrations are under plunging breaking waves, where turbulence generated at the surface may extend to the seafloor, helping to suspend the sediment and mix it upward (Aagaard and Hughes, 2010; Scott et al., 2009; Ting and Nelson, 2011; Yoon and Cox, 2012). Sediment concentrations are more uniform throughout the water column under plunging waves, and therefore surface concentrations are higher than for other types of breaking waves (Wang et al., 2002). Theoretical methods for calculating sediment

concentrations under plunging waves are inaccurate in the swash and surf zones (Aagaard and Jensen, 2013; Kana, 1978), and the maximum observed values of sediment concentration under plunging breakers are 10 to 100 kg/m^3, depending on water depth (Aagaard and Jensen, 2013). This does not preclude the possibility that sufficient concentrations occurred during the oiling interval (1-May-2010 to 1-September-2010), because data are limited for plunging breakers, are not available from the northern Gulf of Mexico, and do not include observations for offshore wave conditions as large as those calculated in the wave scenarios (empirical study maximum wave height of 2.5 m in 6 m of water depth).

We identified likely conditions for plunging waves using the Iribarren number (ξ_b), calculated as a function of local beach slope (S), breaking wave height (H_b), and deepwater wavelength (L_∞) as (Komar, 1998)

$$\xi_b = \frac{S}{\left(H_b / L_\infty \right)^{1/2}} \tag{2}$$

Spilling breakers have ξ_b < 0.4; plunging breakers have 0.4 < ξ_b < 2.0; and surging breakers have ξ_b > 2.0.

Because sediment suspension in the surf zone is primarily driven by breaker-induced turbulence, it is generally accepted that sediment concentration and transport will vary with wave-breaking dissipation (Dean, 1977; Larson et al., 1990). It was therefore assumed that for surface suspended sediment to reach the 200 kg/m^3 concentration required to form an agglomerate, a certain threshold of wave breaking dissipation was required. Due to a lack of empirical data on agglomerate formation, we used here an order of magnitude estimate based on a methodology to estimate changes in cross-shore bathymetry profiles. Dean (1977) extended the Bruun Rule (Per Bruun,1954) concept of an equilibrium nearshore cross-shore profile based on incident wave conditions. The equilibrium dissipation per unit volume (D_*) is a function of the breaker index (γ , the ratio of wave height to water depth at which

waves will break, commonly taken as 0.78), the density of water (ρ_W, 1027 kg/m^3), acceleration due to gravity (g, 9.8 m/s^2), and a scaling parameter (A, units of m$^{1/3}$) that determines the shape of the cross-shore profile (presented in Wang and Kraus, 2005).

$$D_* = \frac{5}{24}\gamma^2 \rho_w g^{3/2} A^{3/2} \quad (3)$$

A varies with sediment grain size. For 0.3-mm diameter sand, the size used in estimating burial and exhumation of SRBs (Plant et al., 2013), empirical and theoretical estimates of A range from 0.05-0.1 m$^{1/3}$ (Dean, 1991), producing D_* values of 45-126 W/m^3. D_* has been used in numerical models to specify the threshold at which cross-shore sediment transport will occur (Larson et al., 1990). Here, it was used as an estimate of the energy required to produce the suspended sediment concentrations needed to form an agglomerate, and was taken as 50 W/m^3. The numerical wave model provided the dissipation per unit horizontal area (units of W/m^2), therefore D_* was multiplied by the model depth to provide the (depth-variant) threshold of model output dissipation required. At a depth of 1 m, the threshold was 50 W/m^2; this value was taken as a uniform threshold throughout the domain, providing a conservative (low) estimate of the dissipation needed to suspend sufficient sediment for agglomerate formation.

In summary, we concluded that the most likely conditions for agglomerate formation were when (1) plunging waves were present (Iribarren numbers between 0.4 and 2) and (2) wave-breaking dissipation reached or exceeded 50 W/m^3. We used the output of a wave model to identify times and places where these conditions may have occurred, as discussed below.

Methods

A numerical model was used to simulate spatially varying wave conditions along the Alabama and western Florida coast (Figure 1) in a set of 80 wave scenarios discretized by wave height and direction (

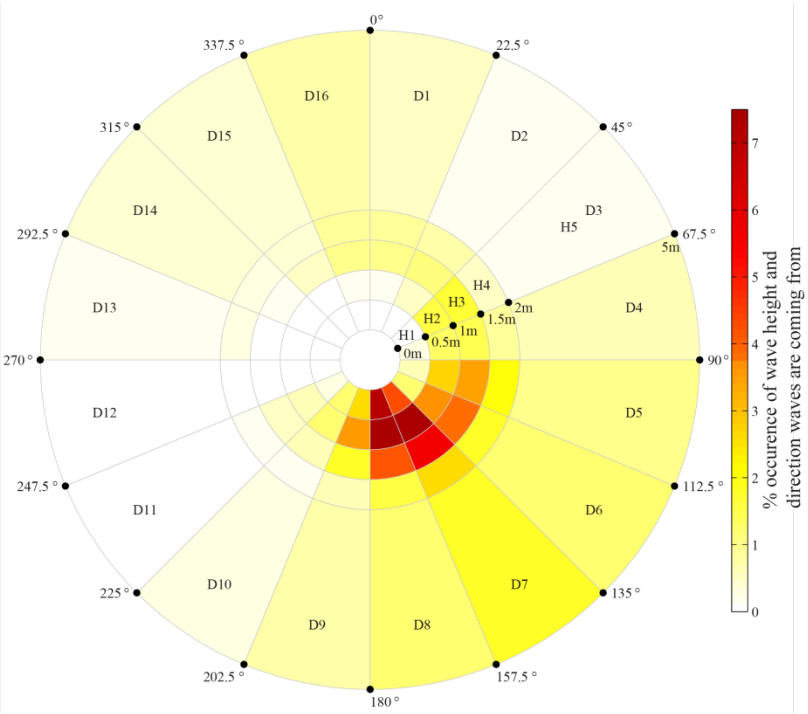

Figure 2) as documented in Plant et al. (2013). These scenarios were used to identify the range of water depths where plunging-wave conditions may have mixed oil with suspended sediment to form agglomerates. The conditions conducive for agglomerate formation are described in the first section, with subheading *Depth of Wave Breaking*. The methodology by which the corresponding water depths can be converted to cross-shore locations using pre-oiling bathymetry and a time series of water level variation is described in *Water Level Variation over Oiling Interval*.

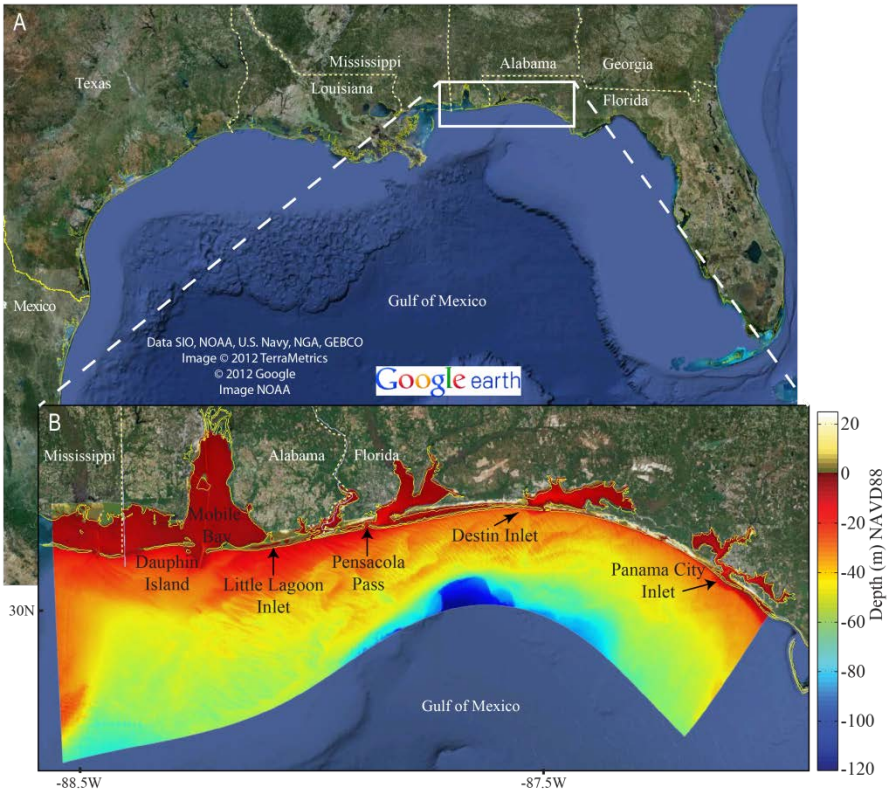

Figure 1. Numerical model domain for the Alabama and western Florida coasts. Modified from Plant et al, 2013.

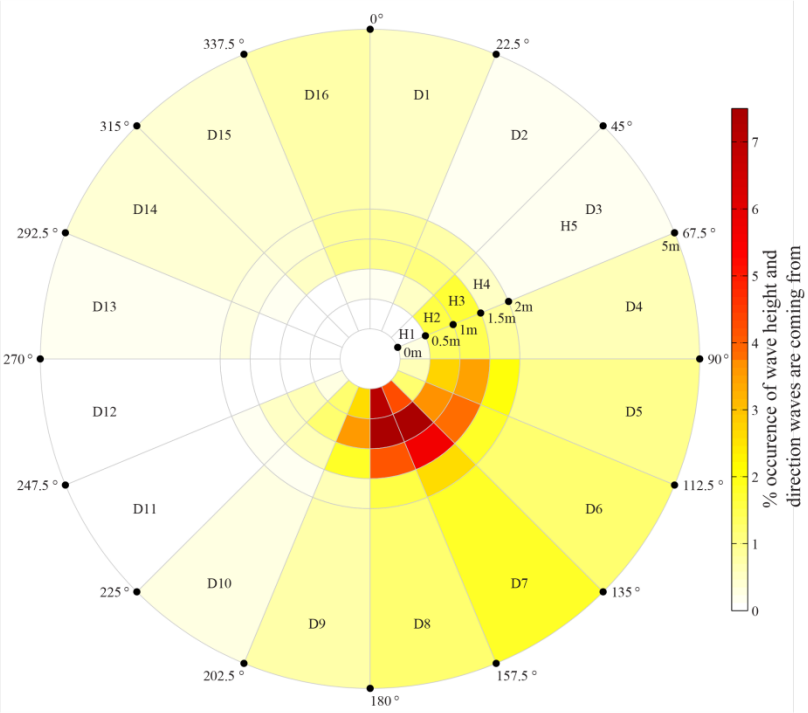

Figure 2. Bins defining the 80 wave scenarios used to characterize offshore wave conditions. Use of wave scenarios has been shown to accurately capture onshore wave conditions (Plant et al., 2013) while reducing computational expense. Wave data were from National Oceanic and Atmospheric Administration (NOAA) buoy 42040 over the oiling interval (1-May-2010 to 1-September-2010), and were characterized as belonging to one of the 80 illustrated scenario bins based on significant wave height and incident wave direction. From Plant et al., 2013.

Depth of Wave Breaking

Depths at which agglomerates may have formed were calculated by identifying (1) locations of energetic wave breaking (e.g., high wave energy dissipation); and (2) locations where plunging breaker conditions existed. The wave simulations, performed with Delft3D-WAVE and presented in Plant et al. (2013), included calculations of dissipation due to depth-induced wave breaking. This spatially variant wave-breaking dissipation parameter was output for each of the 80 scenarios. Using the bathymetry and wave simulation outputs, the Iribarren number (equation 2) was calculated for those locations where

dissipation due to depth-induced wave breaking was greater than zero, and was used to determine the spatial distribution of plunging breakers.

We identified the scenarios that corresponded to time variant conditions in the Gulf of Mexico by matching scenario parameters (offshore wave height and direction) with time series of wave-model output from Wavewatch III. Wavewatch III is an operational wave model with 4-minute spatial resolution run by NOAA. The "best-match scenario" (Plant et al, 2013), i.e., the scenario most closely matching Wavewatch III output conditions at the location of NOAA buoy 42040, was identified for each 3-hourly time step during the oiling interval (1-May-2010 to 1-September-2010). Wavewatch III model output was used rather than wave buoy observations to avoid gaps in time when the wave buoy was not reporting data, and compares well to buoy observations with a root-mean square error of less than 0.25 m (see Plant et al, 2013). Using this time series, we determined the cross-shore distribution of the percentage of time plunging breakers occurred over the oiling interval, as well the cross-shore location of the strongest energy dissipation (e.g., primary breaker depth), at each alongshore location. We then determined the variation in these parameters with depth.

Water Level Variation over Oiling interval

Water depth in the Gulf of Mexico varies on time scales of hours to days, due to tides and subtidal oscillations in water level caused by winds and the dynamic sea-surface topography associated with large-scale waves and circulation. These fluctuations were not incorporated in the wave scenarios described above, which were run as stationary cases with fixed offshore water level. In this section, we describe our procedures for estimating time series of water-level fluctuations at each longitudinal location. These may be used in the future to adjust estimates of the offshore extent of possible agglomerate formation depths calculated in this appendix.

Archived model results from the HYbrid Coordinate Ocean Model (HYCOM, http://hycom.org/dataserver/goml0pt04) output were used to evaluate low-frequency water-level fluctuations. This model, which does not include tides, provided hourly estimates of water levels in the Gulf of Mexico at a resolution of approximately 4 km. Model output was nominally referenced to mean sea level. However, we found persistent differences between modeled water levels and data from the two tide gauges (Dauphin Island, AL, and Panama City, FL) within our domain at locations resolved by HYCOM. To correct the model output for these differences, the observed water levels were low-pass filtered to remove tidal fluctuations, and for each tide gauge the difference between the subtidal observed water level and the HYCOM prediction in the nearest grid cell was calculated. The time-varying difference averaged over the two tide gauges was calculated and applied as a correction to the HYCOM water levels. Because the Dauphin Island gauge is located near the western boundary of our domain and the Panama City gauge is located toward the eastern boundary, this average correction was assumed to be a good estimate over our region of interest and was applied as a spatially uniform value throughout the model domain.

The ADCIRC tidal database (http://adcirc.org/products/adcirc-tidal-databases/) was used to account for tidally-induced water level variation. This model provided spatially resolved estimates of the amplitude and phase of the M2, S2, N2, K2, O1, K1, Q1, M4, M6, and STEADY model constituents. These constituents were used to develop a time-series of tidal water level variations over the oiling interval in each grid cell in the model domain. The ADCIRC database does not include longer-period tides such as the annual and semi-annual tide, but the associated water-level fluctuations were included in the tide gauge-corrected HYCOM data.

The tidal and subtidal water level variations were combined to form spatially variant time-series of water level during the oiling interval. These may later be combined with bathymetry and depths of possible agglomerate formation to identify the cross-shore locations of possible SOMS.

Results

The numerical wave model scenarios were used to spatially and temporally resolve conditions of wave breaking. These model outputs, combined with archived models of low-frequency and tidal water level variation, provided the information needed to convert depths of possible agglomerate formation to cross-shore locations. The analysis of water depth of possible agglomerate formation, characterized by both wave breaking energy and breaker type, is described in *Identified Depths of Wave Breaking*. The variability of water depth over the oiling interval with tides and low-frequency processes such as storms is found in *Estimation of Water Levels.*

Identified Depths of Wave Breaking

The primary breaker depth was determined as the point of maximum wave-energy dissipation in the surf zone (Figure 3). Scenarios with the highest wave heights, and particularly those with waves coming from offshore, had deeper breaking depths scenarios with smaller wave heights. Primary breaker depths generally varied from a few cm to less than 2-3 m, with a few scenarios producing deeper wave-breaking depths (up to 5 m) for the largest offshore wave heights. The deepest wave breaking depths corresponded to scenario 73, with offshore wave heights of 2.0+ m coming from a direction of 180°-202.5°. This scenario portrayed wave conditions that included tropical storms and hurricanes in the Gulf of Mexico. For the oiling interval considered here, that included the far-field passing of Hurricane Alex in late June/early July 2010 and the mid-July 2010 near-field passing of Tropical Storm Bonnie.

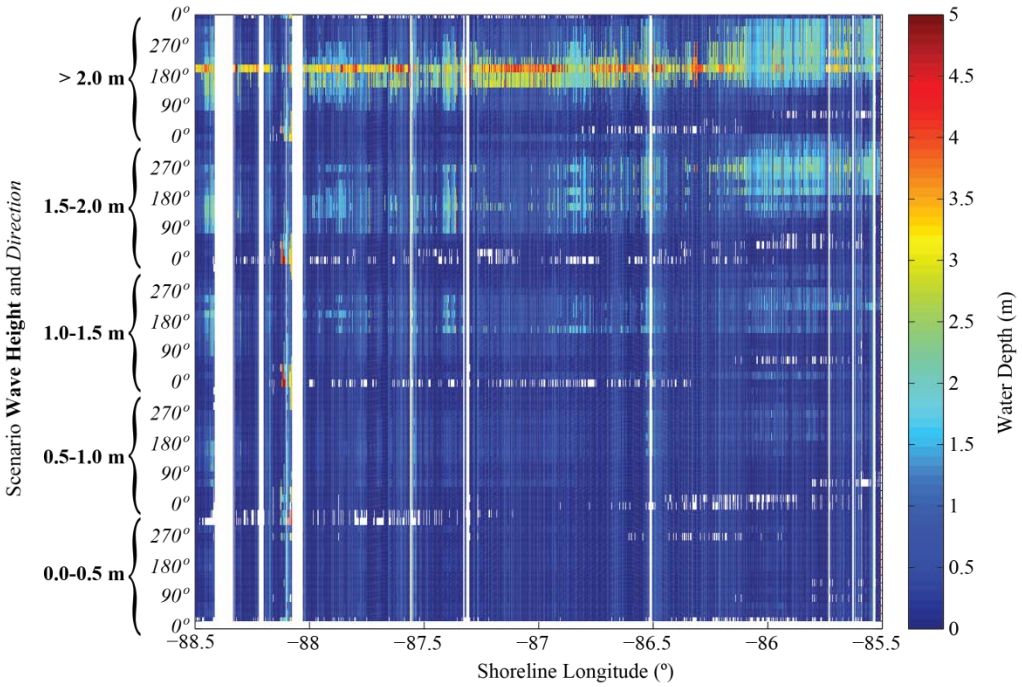

Figure 3. Depth of maximum wave energy dissipation due to breaking at each alongshore location and for each of the 80 numerical wave model scenarios defined by wave height (m) and the incident wave direction (degrees relative to north, direction waves are coming from; figure 2). Gaps in the results correspond to alongshore locations of inlets and breaks between barrier islands. For the larger wave scenarios (offshore significant wave height > 2.0 m), the depth of maximum wave energy dissipation is up to 5 m, decreasing with decreasing offshore wave height.

Using the Iribarren number (Equation 2), the depth at the onset of plunging breakers was identified (Figure 4). Iribarren number was calculated using model bathymetry and output values of significant wave height and wavelength at those locations where the dissipation due to wave breaking was greater than zero. Under low energy wave conditions, plunging breakers occured at the shore-break, whereas when the offshore wave height was over 1.0 m plunging breakers occurred over sand bars at some alongshore locations (depths 6-10 m).

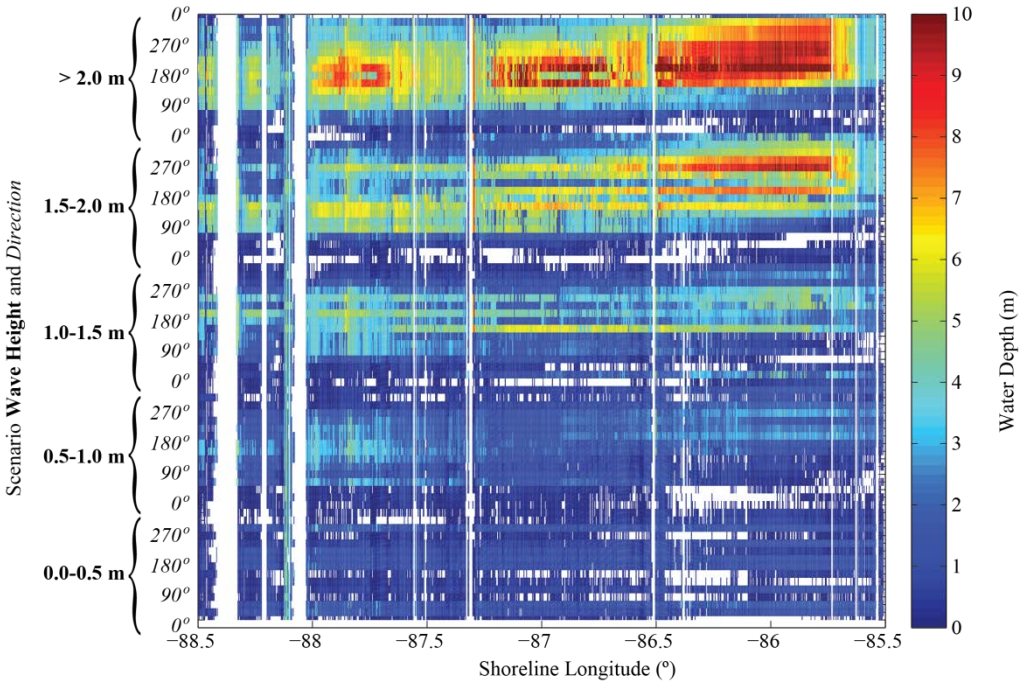

Figure 4. Plunging breaker depths, as indicated by the Iribarren numbers and dissipation greater than zero. Gaps indicate the criterion for plunging breakers was not met at any depth in the profile for that numerical wave model scenario, or that the location was offshore of an inlet or break in the barrier islands. For offshore wave heights of greater than 1.5 m, plunging breaker depth in some location can be up to 10 m, decreasing with decreasing offshore wave height.

The depth of plunging breakers with energy dissipation greater than 50 W/m^2 was used to identify depths with both plunging waves and high energy for mixing sand and oil (Figure 5). The depths that satisfied both criteria were shallower than the depths identified by the plunging breaker criterion alone. For offshore wave heights of less than 1.0 m, plunging breakers rarely occurred with dissipation above 50 W/m^2 and, for all but the highest wave scenarios, these conditions were confined to depths shallower than 2-3 m. For the tropical storm cases, the maximum water depth of plunging breakers with dissipation greater than 50 W/m^2 was 6-7 m.

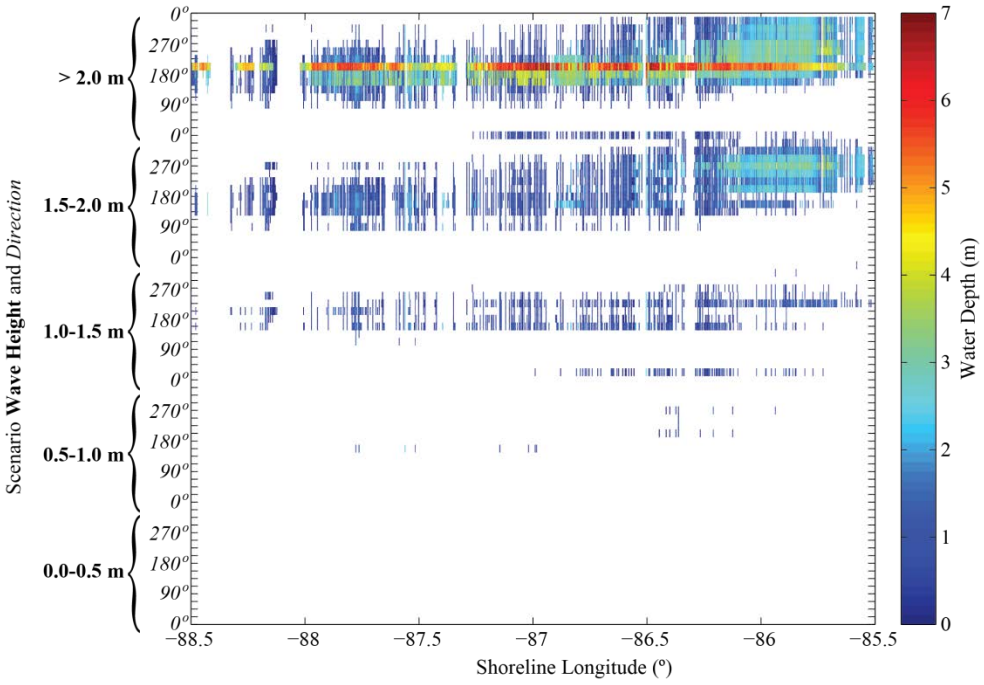

Figure 5. Plunging breaker depths with a dissipation exceeding 50 W/m^2. Gaps indicate the criterion for plunging breakers or the dissipation threshold of 50 W/m^2 was not exceeded in the profile for that scenario. The deepest plunging breaker depths (figure 4) generally corresponded to wave energy dissipation of 50 W/m^2. Incorporating this minimum value as a second criterion representing the minimum energy dissipation required to form an agglomerate reduced the maximum plunging breaker depth to less than 7 m for all scenarios.

Time series of breaker depths at each spatial location were created by using wave-model output for the best-match scenarios described previously in the Methods – Depth of Wave Breaking section. Statistics of the time series describe the range of primary breaker depths at each location (Figure 6). These depths did not include water level variation, which is addressed below in *Estimation of Water Level Variation*. Breaking typically occurred in shallow depths (< 1 m) due to the prevalence of low-energy wave conditions in the northern Gulf of Mexico. Breaking extended to depths of 4-6 m under storm conditions with higher, longer-periods waves. The deepest primary breaker depths (maximum depths in Figure 6), were associated with Hurricane Alex (late June/early July) or Tropical Storm Bonnie (mid July).

If oil was not present at a given location during those periods, the offshore limits of agglomerate formation associated with primary breaker depth would have been closer to the mean value.

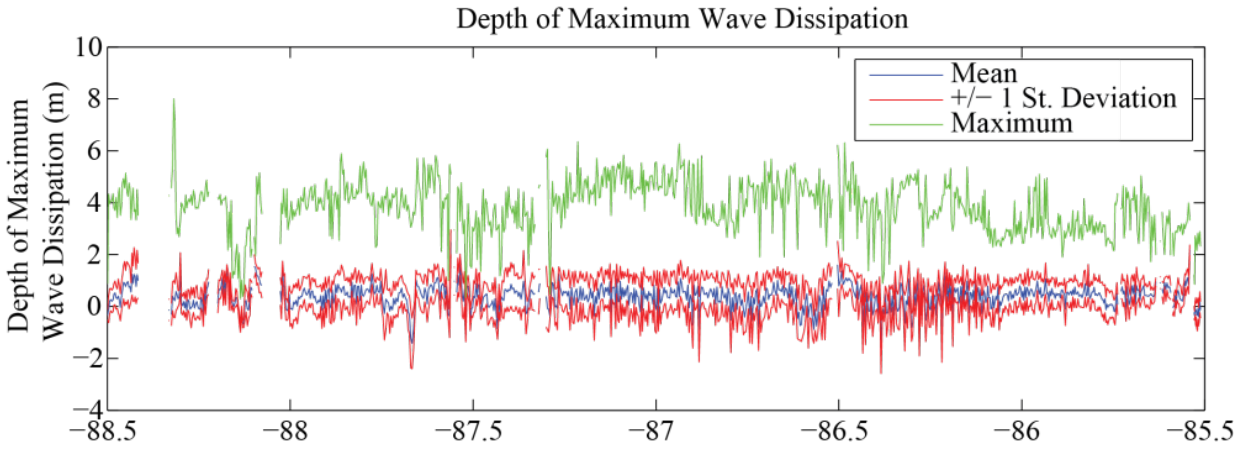

Figure 6. Alongshore-variant primary breaker depth using scenario-based numerical model output for the oiling interval, 01-May-2010 to 01-September-2010. Shown is the mean value +/- one standard deviation, and the maximum value defined by offshore tropical storm conditions. Under most wave conditions (within one standard deviation of the mean), the depth of maximum wave dissipation was less than 2 m.

Time-series of the plunging breaker depths were created from the wave-model output. The alongshore extent of the model was subdivided into six sections, delineated by inlets, to isolate regions where it was assumed the distribution of surface oil in the surf zone likely varied due interaction with inlet hydrodynamics. The percentage of the oiling interval during which plunging breakers occurred as a function of water depth was calculated for each section (Figure 7). The percentage of time plunging breakers occurred decreased with increasing water depth. With the exception of the Little Lagoon to Perdido Pass and Destin to Panama City segments, plunging breaker conditions occurred less than 5% of the time at depths less than 2 m. The percentage of the oiling interval during which plunging breakers occurred and the threshold of 50 W/m^2 was exceeded (conditions for agglomerate formation) was smaller, dropping to 1-2% of the oiling interval for all depths (Figure 7, shown in red).

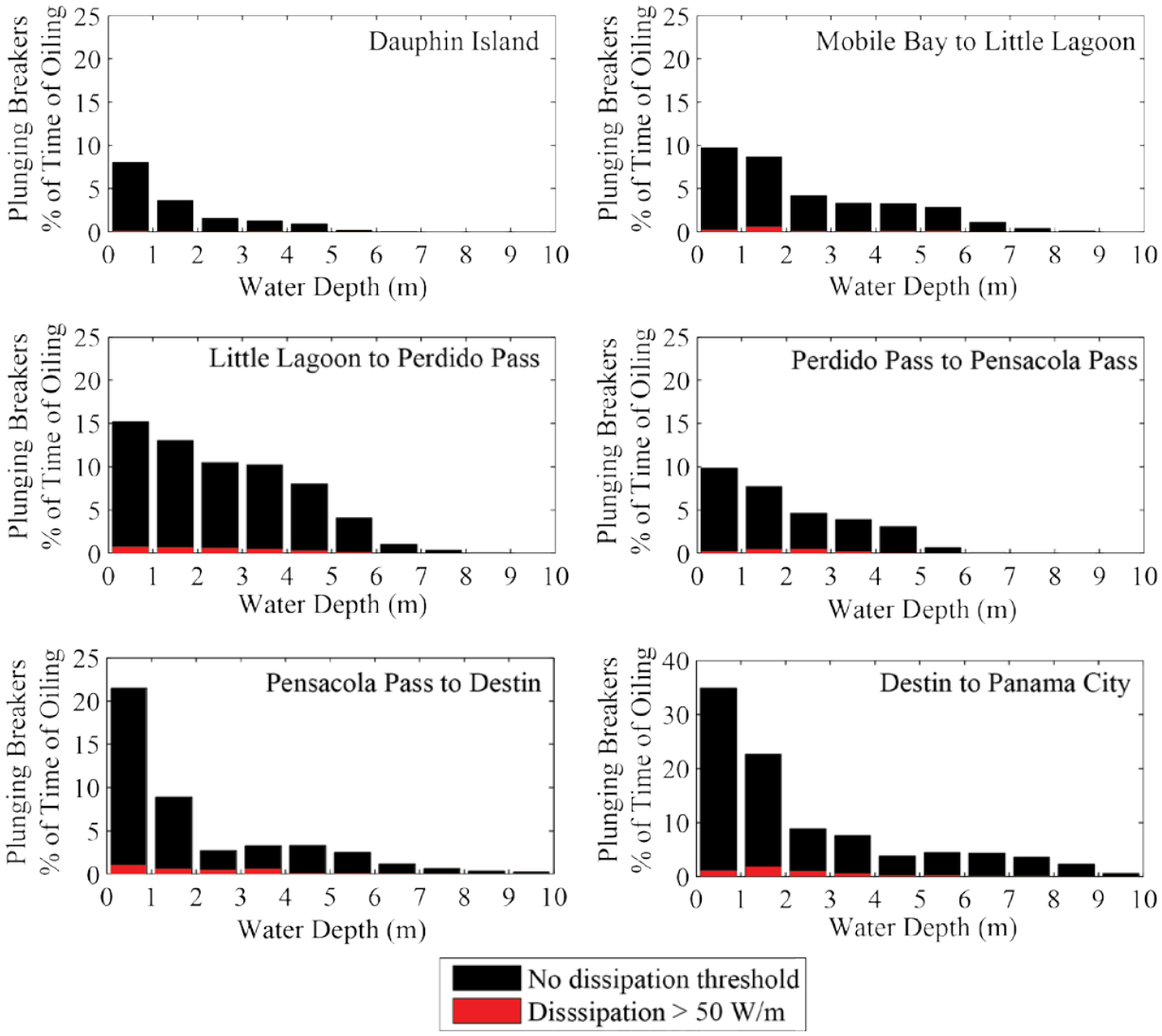

Figure 7. Percentage of time during the oiling interval, taken as 01-May-2010 to 01-September-2010, for which plunging breaker conditions occurred as a function of depth. Locations of the alongshore delineations are shown in Figure 1. Plunging breakers most often occurred in shallow depths of less than 1-2 m in all locations, occasionally occurring at depths of up to 10 m. With the addition of a minimum wave energy dissipation of 50 W/m, representing the minimum energy needed for agglomerate formation, plunging breaker depths meeting this second criterion occurred less than 1-2% of the oiling interval at all depths.

Based on the theoretically and empirically based assumption that energetic wave breaking was required for agglomerate formation, we also analyzed the percentage of the oiling interval for which all three criteria were met (i.e., plunging breakers with energy dissipation greater than 50 W/m^2 occurred at the

primary breaker depth). Even in shallow depths of less than 1 m, plunging breakers with dissipation energy of greater than 50 W/m^2 at the primary breaker depth occurred less than 0.2% of the oiling interval.

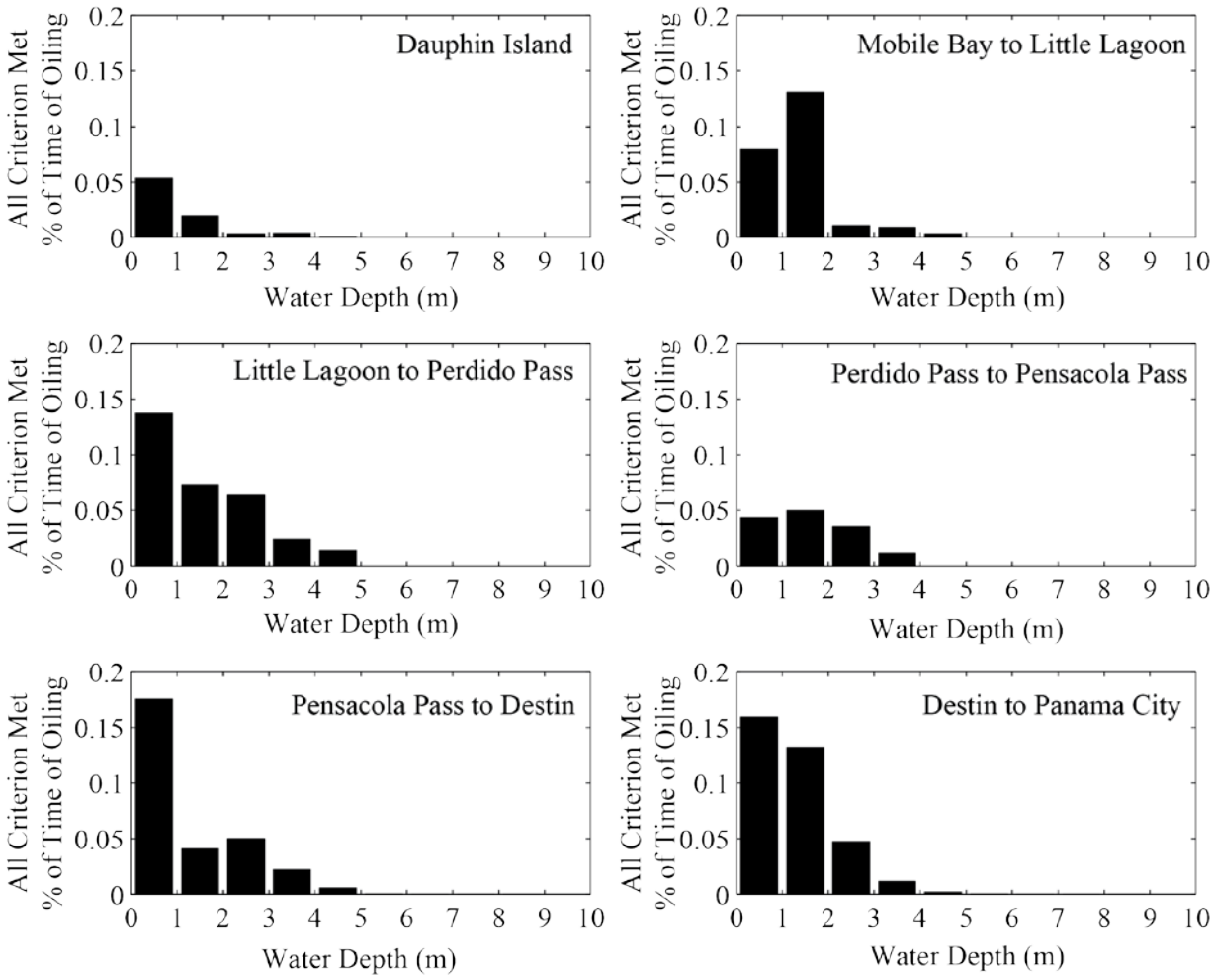

Figure 8. Percentage of time during the oiling interval, taken as 01-May-2010 to 01-September-2010, for which plunging breakers with dissipation greater than 50 W/m^2 occurred at the primary breaker line. These criteria were met less than 0.2% of the oiling interval at all depths. Locations of the alongshore delineations are shown in Figure 1. These depths were where agglomerates could have formed, based on the theoretically and empirically based assumption that energetic wave breaking was required for agglomerate formation.

Estimation of Water Levels

An offset of between 5-35 cm was found (Figure 9) when HYCOM estimates of water level were compared to tide gauge observations at Dauphin Island and Panama City. Although the difference between the model and the gauges varied in time, the magnitude of the error was similar between the two gauges (Dauphin Island and Panama City), indicating that the offset was the result of a large-scale difference in the HYCOM model relative to the tide gauge data and not associated with smaller-scale water level variations associated with the individual tide gauges. For this reason, we used a time-variant water level correction, taken as the mean difference of the two tide gauges at each time, applied over the entire model domain.

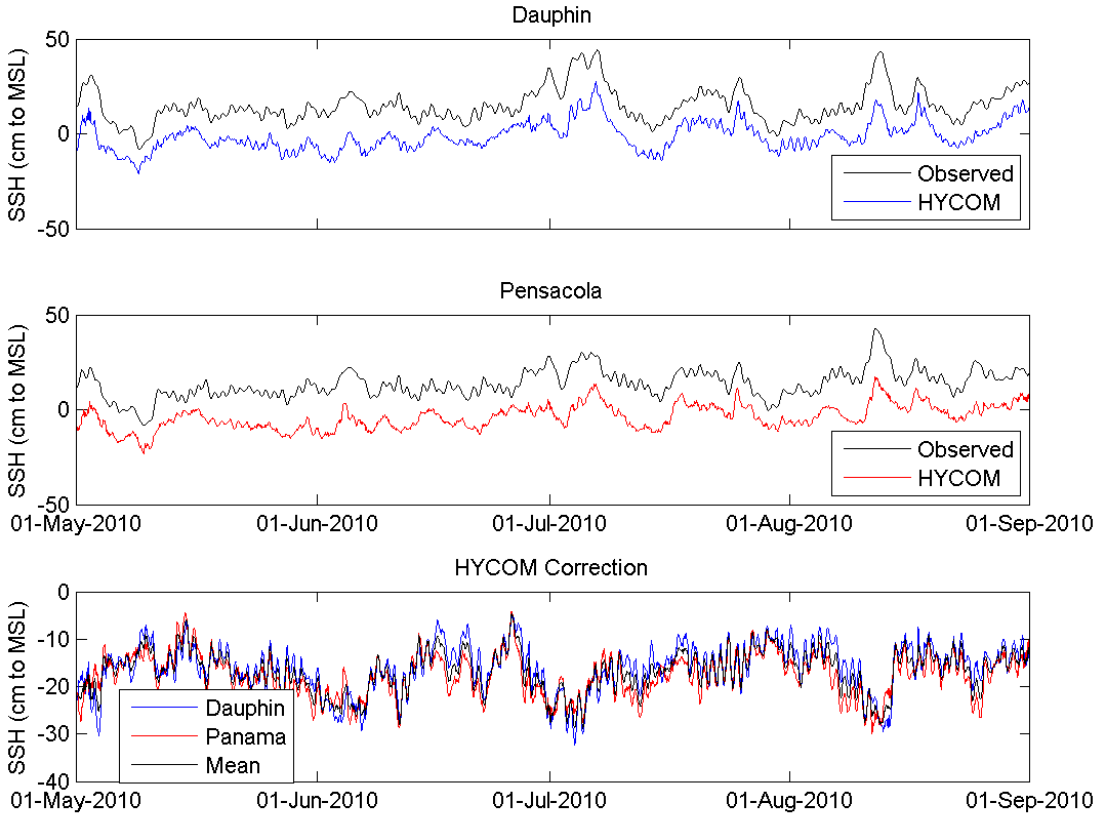

Figure 9: Comparison of HYCOM water levels to low-pass filtered tide gauge water levels, showing a time-variant offset between the observed tide gauge data and model output. Because the offset was consistent at any given time between the two tide gauges and they are located near the western and eastern extent of the model domain, respectively, the offset was assumed to be spatially uniform over the model domain. A spatially uniform time-variant correction calculated as the average difference between the two tide gauges and model output at each point in time was applied to water level output from HYCOM.

After we reconstructed tidal water level variation over the model domain during the oiling interval using the ADCIRC tidal constituent database, we compared it to observed water levels at the Dauphin Island and Panama City tide gauges. To isolate the tidally variant component, the corrected HYCOM low-frequency time series was subtracted from the observed water level time series before comparison to

the ADCIRC reconstruction. The reconstruction adequately captured the tidal variation in water level, noting that the ADCIRC database only contains a subset of all tidal constituents.

The time-series of tidally variant water levels and low-frequency water levels were combined to reconstruct the full time-series of water level variation. At the Dauphin Island and Panama City tide gauges, the reconstructions were assessed by comparing them to observed water levels (Figure 10). The root mean square error was between 4.5-5.5 cm at the two gauges, with a bias of < 2 cm and an R^2 of > 0.9, indicating that the water level variations at the two gauges were modeled well by the reconstruction (Table 1). Because the gauges are located at opposite ends of the model domain, this result indicated that water level reconstructions of large-scale variability were modeled well throughout the domain.

Table 1. Comparison of reconstructed water level variation with observations at the Dauphin Island and Panama City tide gauges. RMSE is the root mean square error. Including tidal variation, lower-frequency oscillations captured by HYCOM, and the temporally variant HYCOM water level offset correction (figure 9), the water level reconstructed from numerical model output compares well to observed data from the two tide gauges within the model domain.

Gauge	RMSE	Bias	R^2
Dauphin Island	4.6 cm	-2.0 cm	0.93
Panama City	5.4 cm	0.6 cm	0.90

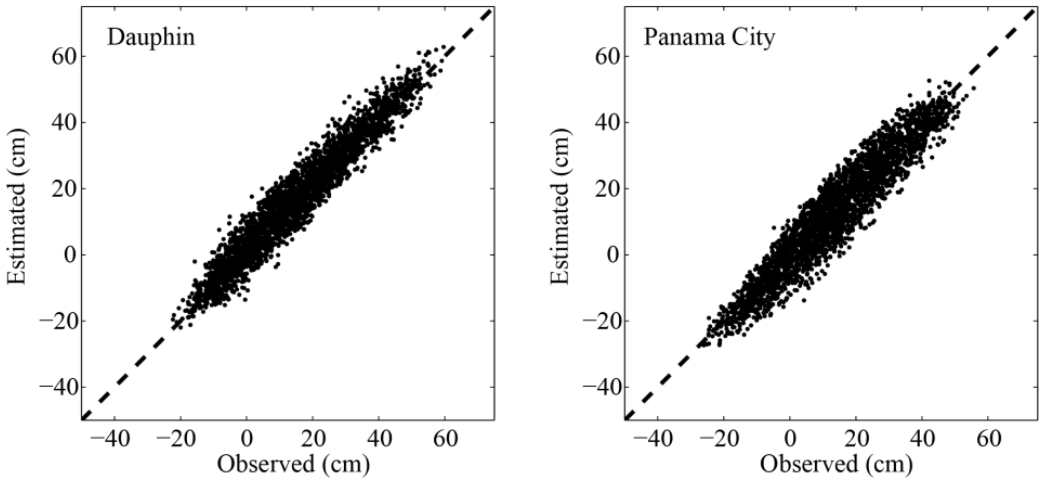

Figure 10: Comparison of observed water levels and HYCOM/ADCIRC-based reconstructed estimates of water level variations over the oiling interval at the Dauphin Island, AL, and Panama City, FL, tide gauges. The reconstructed water level matches well with observations, indicating the reconstruction method adequately captures water level variation over the oiling interval.

The water level model output was used to produce a time-stack of the spatial and temporal variation in water level across our domain. The maximum and minimum water levels provide boundaries of the depth variation during the oiling interval at any given location. The tidal and subtidal water level processes, such as storm surge, produced water levels as low as -20 cm below mean water level and as high as 60 cm above mean water level. By adding these spatially variant minimum and maximum water levels to pre-oiling bathymetry, the range of water depths during the oiling interval can be identified. A diagram of the methodology for using water depth variation, bathymetry, and possible agglomerate formation depth to identify at any particular alongshore location the cross-shore range over which oil mats may have formed is shown in Figure 11. Those cross-shore locations where the range of depths during the oiling interval (highest and lowest water level shown in diagram) cross through the depths of possible agglomerate formation as described above (single depth of agglomerate formation shown in diagram, h_A) are sites where oil mats may have formed, and a subset of those sites, where the beach

profile accreted post-oiling and has not eroded back to pre-oiling depths, are the possible locations of SOMs.

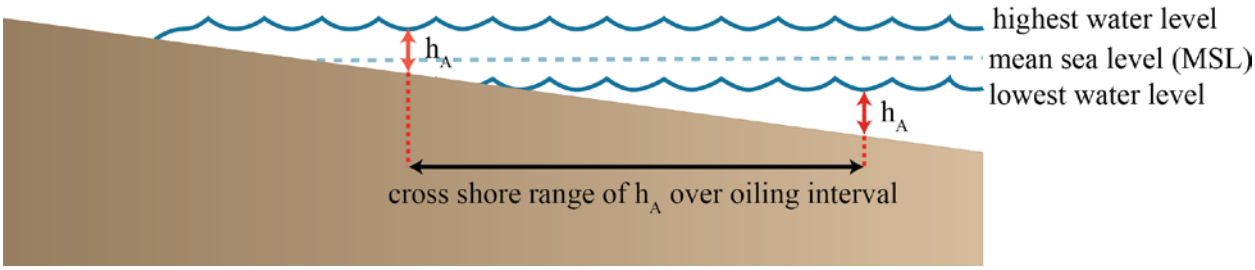

Figure 11. Diagram of method for using water level variation, bathymetry, and depth of possible agglomerate formation (h_A) at a particular alongshore location to identify the cross-shore range over which oil agglomerates may remain deposited in the nearshore sediments.

Discussion: Sources of Uncertainty

The approach outlined above has several sources of uncertainty, particularly given the lack of empirical studies on agglomerate formation dynamics. The Iribarren number, used to distinguish breaker type, is sensitive to the local beach slope. This value may have varied, particularly in the highly dynamic surf zone, from values in the model bathymetry used here. The Iribarren number uses a single, dominant wave period to characterize the relevant wave length and does not consider the full spectrum of incident waves of various height and direction (Komar, 1998). We have used the primary breaker depth as a metric of possible agglomerate formation, whereas it is possible that some threshold of dissipation not necessarily associated with the cross-shore peak in breaking is a better metric of agglomerate formation. Depending on its value, a dissipation threshold could, under higher wave conditions, be exceeded offshore of the primary breaker depth. Under lower energy wave conditions, this threshold might not be exceeded anywhere in the nearshore. Based on a theoretical threshold of energy dissipation required for initiation of cross-shore sediment transport and using it as a proxy for the concentration of sediment suspension required to induce oil and sediment agglomerate formation and

sinking of globules to the seabed, we used a dissipation threshold of 50 W/m^2 in conjunction with plunging breakers to assess the possible depths of agglomerate formation. Without empirical data, the appropriate value to use for this threshold was uncertain; however, because it was based on conservative estimates of the controlling parameters in a depth of 1 m, the actual dissipation threshold at depths of greater than 1 m is most likely higher.

The unknown mechanics of sand/oil mixing also introduced uncertainty. We have assumed that agglomerate formation occurs instantaneously if the surface concentration of sediment was sufficient for the resultant agglomerate to sink. The agglomerate formation process may require concentrations above this threshold for some finite amount of time that was impossible to quantify without empirical studies. In addition, mat formation was a complex process, and required the mixing of additional sand into the agglomerate over neutral buoyancy, likely after the agglomerate reached the seafloor, in order to create a stable mass that adhered to the bottom. Conversely, at lower concentrations sediment may have gradually accumulated until negative buoyancy was achieved, a process that also could not be quantified without additional empirically-based research. The possibility of shell hash, organic material, or other substances mixing with residue oil was not considered here, and would alter the agglomerate density.

As a final note, because the exact location of oil slicks during the oiling interval was unknown, the analysis presented here indicates locations where agglomerates may have possibly formed at the surface, and does not address if/where they actually formed (e.g., where/when oil was present in conjunction with sufficient sediment concentrations at the surface). In addition, the possibility of agglomerates being transported cross-shore or alongshore while sinking to or upon reaching the seafloor was not considered here.

Conclusions

To determine conditions under which sinking sand/oil agglomerates may have formed and sunk to the seafloor, we used theoretical and empirical analysis of the surface suspended sediment concentrations under non-breaking wave conditions offshore of Alabama and the west coast of Florida to compare to the concentrations of sand and oil required for agglomerates to sink. We determined that without the turbulence and convective mixing resulting from breaking waves, shoaling waves would be unable to suspend sufficient sediment to the water's surface. Therefore, mats likely formed either in (1) the swash and very shallow nearshore, where shallow water depths allowed surface oil to come in direct contact with the seafloor/beach; or (2) regions of highly energetic wave breaking, where plunging breakers produced intensive convective mixing.

The percentage of time plunging wave conditions occurred was on average less than 10% of the oiling interval (01-May-2010 to 01-September-2010) at depths greater than 2 m. If, in addition to plunging wave conditions, an energy dissipation threshold of 50 W/m^2 was applied to achieve the required level of turbulence, then the percentage of time possible agglomerate formation conditions occurred decreased to less than 2% of the oiling interval at all depths. Given the energetic wave conditions required for agglomerate formation, the primary breaker depth was also identified. Over the oiling interval, the mean depth of the primary breaker depth was in less than 1 m of water depth throughout the model domain, extending out to 4-6 m during tropical storm conditions. If all three criteria were imposed, i.e., plunging waves at the primary breaker depth with dissipation greater than 50 W/m^2, conditions were met less than 0.2% of the oiling interval at all depths. The threshold of 50 W/m^2 was based on an estimate of the dissipation required to initiate cross-shore sediment transport, and was used as a proxy for estimating the dissipation required to suspend sufficient sediment to the surface to form an agglomerate that would start to sink to the seafloor. Because the value was based on

conservative estimates of the underlying parameters, including a depth of calculation of 1 m, it is likely the actual dissipation threshold was higher.

Because the primary interest was the cross-shore location of SOMs, a method was needed to translate the depths of possible agglomerate formation to the cross-shore location where they may have formed. To address this need, the range in water level variability over the time of oiling due to tidal and subtidal processes was identified. Combined with analysis of possible depths of agglomerate formation and pre-oiling bathymetry, the potential cross-shore locations of possible SOMs can be identified.

NOTE: Any use of trade, firm, or product names is for descriptive purposes only and does not imply endorsement by the U.S. Government.

References

Aagaard, T., Hughes, M.G. (2010). Breaker vortices and sediment suspension in the surf zone. *Mar. Geo.* (271), 250-259.

Aagaard, T., Jensen, S.G. (2013). Sediment concentration and vertical mixing under breaking waves. *Mar. Geo.* (336), 146-159.

Dean, R.G. (1977). *Equilibrium Beach Profiles: U.S. Atlantic and Gulf Coasts*, Department of Civil Engineering, Ocean Engineering Report No. 12, University of Delaware, Newark, DE.

Dean, R.G. (1991). Equilibrium beach profiles: Characteristics and applications. *J. Coast. Res.* (7), 53-84.

Grant, W.D., Madsen, O.S. (1982). Movable bed roughness in unsteady oscillatory flow. *J. Geophys. Res.* (87), 469-481.

Kana, T. (1978). Surf zone measurements of suspended sediment. *Proc. 16th Coast. Engr. Conf.*, American Society of Civil Engineers, 1725-1743.

Komar, P. (1998). *Beach processes and Sedimentation*. Prentice-Hall Inc.: Upper Saddle River, 544 pp.

Larson, M., Kraus, N. C., Byrnes, M. R. (1990). SBEACH: Numerical Model for Simulating Storm-Induced Beach Change. Report 2. Numerical Formulation and Model Tests (No. CERC/TR-89-9). COASTAL ENGINEERING RESEARCH CENTER VICKSBURG MS.

Nielson, P. (1992). *Coastal Bottom Boundary Layers and Sediment Transport.* World Scientific Publishing: Singapore. Advanced Series on Ocean Engineering, Vol. 4, 324 pp.

Per Bruun, P. (1954). Coast erosion and the development of beach profiles. Beach Erosion Board Technical Memorandum 44. U.S. Army Corps of Engineers, Washington D.C. 79 pp.

Plant, N.G, Long, J.W., Dalyander, P.S., Thompson, D.M., and Raabe, E.A. (2013). Application of a Hydrodynamic and Sediment Transport Model for Guidance of Response Efforts Related to the Deepwater Horizon Oil Spill in the Northern Gulf of Mexico Along the Coast of Alabama and Florida: U.S. Geological Survey Open-File Report 2012–1234, http://pubs.usgs.gov/of/2012/1234/.

Scott, N.V., Hsu, T.-J., Cox, D. (2009). Steep wave, turbulence, and sediment concentrations statistics beneath and breaking wave field and their implications for sediment transport. *Cont. Shelf Res.* (29), 2303-2317.

Soulsby, R.L. (1997). *Dynamics of Marine Sands*. Thomas Telford Publications: London, 249 pp.

Ting, F.C.K., Nelson, J.R. (2011). Laboratory measurements of large-scale near-bed turbulent flow structures under spilling regular waves. *Coast. Engr.* (58), 151-172.

Wang, P., Ebersole, B.A., Smith, E.R., Johnson, B.D. (2002). Temporal and spatial variations of surf-zone currents and suspended sediment concentration. *Coast. Engr.* (46), 175-211.

Wang, P., Kraus, N.C. (2005). Beach profile equilibrium and patterns of wave decay and energy dissipation across the surf zone elucidated in a large-scale laboratory experiment. *J. Coast. Res.* (21), 522-534.

Yoon, H.-D., Cox, D.T. (2012). Cross-shore variation of intermittent sediment suspension and turbulence induced by depth-limited wave breaking. *Cont. Shelf Res.* (47), 93-106.

Application of Hydrodynamic Models in support of the Buried Oil Project Along the Coast of Louisiana and Mississippi

Prepared in cooperation with the Operational Science Advisory Team (OSAT3) Steering Committee chartered by the Deepwater Horizon Federal On-Scene Coordinator (FOSC)

By Ioannis Y. Georgiou, Zoe J. Hughes

July 13, 2013

Table of Contents

List of Figures

Application of Hydrodynamic Models in support of the Buried Oil Project Along the Coast of Louisiana and Mississippi

By Ioannis Y. Georgiou, and Zoe Hughes

Introduction

Residual oil from the Deepwater Horizon spill can be found in the shallow nearshore in the northern Gulf of Mexico in two primary forms: oil mats and surface residual balls (SRBs). Residual oil mats can be buried beneath sand in the sub-tidal zone or they can be submerged and partly buried in the inner nearshore zone. The mats found in these environments are formed by three primary mechanisms related to oil (emulsified oil called mousse) coming ashore:

1. Oil slicks moved into the swash zone and mixed with sand that was entrained and suspended from seabed by wave swash and backwash on the beachface. The sand and oil slurry formed by this process was deposited in a variety of environments:
   a) stranded in the upper intertidal zone
   b) ponded in the runnels of ridge and runnel systems
   c) buried by sand in the lower intertidal and sub-tidal zones
   d) became attached to lower and subtidal remnant marsh and mangrove exposures
2. Floating oil washed ashore and became stranded by the falling tide. In the warm sun the oil seeped into the sand and stabilized in the upper to lower intertdal zone.

3. The turbulence produced by plunging breaking waves suspended sand from the seabed moving it vertically toward the water surface and mixing it into floating oil. This sand and oil slurry gradually increased in density as more sand was added, eventually reaching a threshold when it became denser than seawater and sank to the bottom.

Due to variability in bottom topography, height of the waves, type of wave, secondary flow interaction, and range in seabed conditions (e.g., existence or absence of bedforms, variability in grain size, presence of shell or organic matter), the concentration and rate of sediment being mixed into the floating oil was non-uniform. Thus, the density threshold at which the sand oil agglomerate sank to the bottom was certainly variable, both spatially and temporally. It is likely that the density threshold occurred on a small scale and globules rather than large agglomerates sank to the bottom. Once reaching the bottom, the globules recombined to form discontinuous and variable dimension agglomerates. As more sediment was added to the agglomerates, mats formed and stabilized to the substrate.

Mats identified along Gulf Coast beaches are generally 1 to 5 m in cross-shore width, meters to tens of meters in alongshore length, and a few to tens of centimeters thick. High energy events, including tropical cyclones, frontal systems, and extratropical storms, exhume buried mats exposing them to breaking waves and increased turbulence. During these events, mats are often disaggregated and chunks and small pieces of mat (surface residue balls; SRBs) are transported onshore and deposited in the supratidal or upper intertidal zones (Shoreline Cleanup and Assessment Team, oral comm., 2012). This report presents the results of a subgroup who developed hydrodynamic and sediment transport models, and who developed techniques for analyzing potential SRB redistribution, burial, and exhumation to provide a better understanding of alongshore processes and movement of SRBs along the coastlines of Mississippi and Louisiana.

Specific Buried Oil Project objectives with respect to hydrodynamic models

To improve understanding and guidance of the Operational Response to shoreline re-oiling, and to support the Operational Science Advisory Team (OSAT3) in further identifying possible locations of buried oil, the following tasks were identified:

- Use existing wave models to determine total wave energy dissipation (surf dissipation and white-capping) for each of the scenarios previously simulated.
- Plot energy versus depth data to establish the maximum conditions where energy dissipation takes place and assess the likelihood of sediment suspension.

- Formulate a framework for identifying potential locations of buried oil based on information determined from tasks one and two above.

To achieve these objectives, the previously developed and validated hydrodynamic models (Georgiou et al., 2013) were used to determine maximum wave dissipation scenarios, rates and volumes of sediment suspension, modes of sediment and oil mixing, and other tasks of this study. The analysis included calculations of wave energy density and the magnitude of the dissipation terms and formulation of energy density (or total energy dissipation) plotted against depth. Results were displayed in histograms showing the mean wave orbital velocity, peak dissipation terms, and the corresponding depth of occurrence.

Methods

The coastline of interest included in this analysis covers the barrier islands of coastal Louisiana, stretching from the Isles Dernieres, Louisiana, east to Mobile Inlet, Alabama. Moreover, the domains of interest and study focus on the barrier islands of Mississippi, mainland Mississippi, and the entire coastline of Louisiana from Isles Dernieres eastward to Pelican Island. Wave models previously developed for OSAT3 (hydrodynamics in support of operations) were utilized. A full description of the theory and application of these models can be found in Appendix 1 of this report and in Georgiou et al (2013). The domain (geographical coverage) of the models for this study is shown in Figure 1. The wave model resolution is constant with 500 m for the offshore model grid, with nested local grids of 75 - 100 m resolution (Georgiou et al., 2013). The nearshore grids were oriented parallel to the local shoreline trend for simplicity, and to avoid stair-stepping effects. We used the Simulating WAves in the Nearshore (SWAN) model, which is a third-generation wave model developed at Delft University of Technology that computes random, short-crested wind-generated waves in coastal regions and inland waters. The SWAN model can account for the following physical conditions:

- Wave propagation in time and space, shoaling, refraction as a function of current and depth, frequency shifting due to currents, and non-stationary depth.
- Wave generation by wind.
- Three- and four-wave interactions.
- White-capping, bottom friction and depth-induced breaking.

- Dissipation caused by vegetation.
- Wave-induced set-up.
- Transmission through and reflection (specular and diffuse) against obstacles.
-

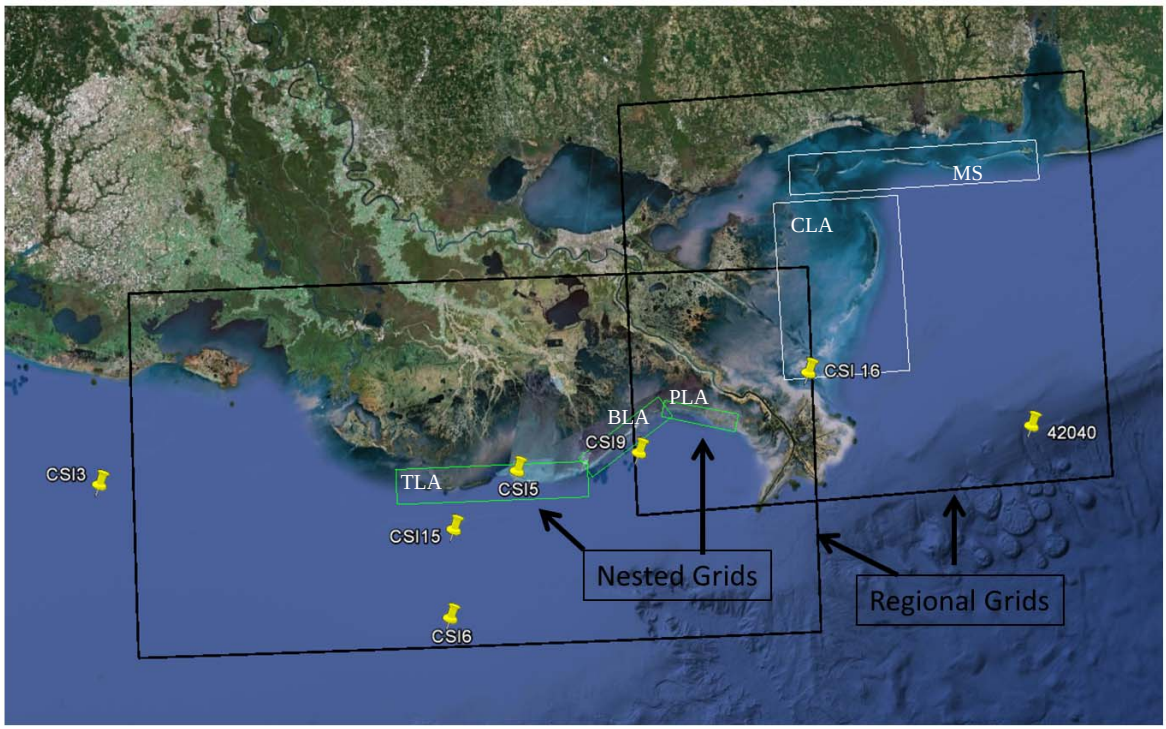

Figure 1. Computational grids for Wave modeling using SWAN; Black rectangles denote regional grids, and green and white rectangles, show the location and extent of the nested grids. Regional grid resolution is 500 m, whereas nested grid resolution is 100 m in LA and 75 m in MS. Also shown are the locations of the NOAA buoy 42040 and CSI locations where additional data for model skill were obtained (from Georgiou et al., 2013).

Approach to analysis and theory

This analysis is based on the hypothesis that submerged oil residue mats (SOM) formed by breaking waves entraining sand into the water column where it mixed with surface oil and eventually reached a density threshold and sunk to the seabed. This hypothesis is consistent with (1) breaking wave processes inducing bottom turbulence and sand suspension as they approach the surfzone, (2) the presence of sandy substrates, and (3) evidence that energy dissipation is concentrated at depths correlating well with known locations of mats.

Waves transform as they approach coastal water by several processes such as shoaling, refraction, diffraction, and breaking. For each of the nearshore nested domains shown in Figure 1 the total energy dissipation is recorded for each cell. The dissipation terms for white-capping (a deepwater dissipation mechanism) and surf dissipation (occurring in nearshore environments) were calculated in the SWAN model (i.e. they are computed for each grid element) using the expression given by Booij et al (1999). The total energy dissipation takes the form of

$$E^{n}{}_{t}(x, y) = E^{n}{}_{surf}(x, y) + E^{n}{}_{whitecapping}(x, y)$$

where *n* is the number of scenario simulations (40 scenarios) and each scenario has $E^{n}{}_{t}(x, y)$ instances of energy dissipation, and (*x*,*y*) is the spatial domain index for each of the nested domains (Figure 1). For each site (e.g., Terrebonne, Barataria, etc.) $E^{n}{}_{t}(x, y)$ was grouped and binned into depth increments of 0.5 m. The objective in this step is to provide a measure of the total energy dissipation within a certain depth range, which most likely coincides with the zone of oil and sediment agglomerate development, globules settling to the bottom, mat formation, and possible mat burial. Theoretically, the energy distribution curve across the depth increments should be normally distributed (Figure 2) where the peaked portion of the curve (shown by the dashed lines) coincides with the depth where energy is most frequently dissipated. The colored circles illustrate bottom orbital velocity associated with each wave energy dissipation term (Figure 2). This can be used to infer bed mobility and the likelihood of sand entrainment. Another way for sand entrainment is through turbulence produced by a breaking wave (particularly plunging wave breaking), when the breaking crest imparts its force on the seabed. The analysis herein directly addresses the first process although only indirectly addresses processes associated with the second method of energy dissipation.

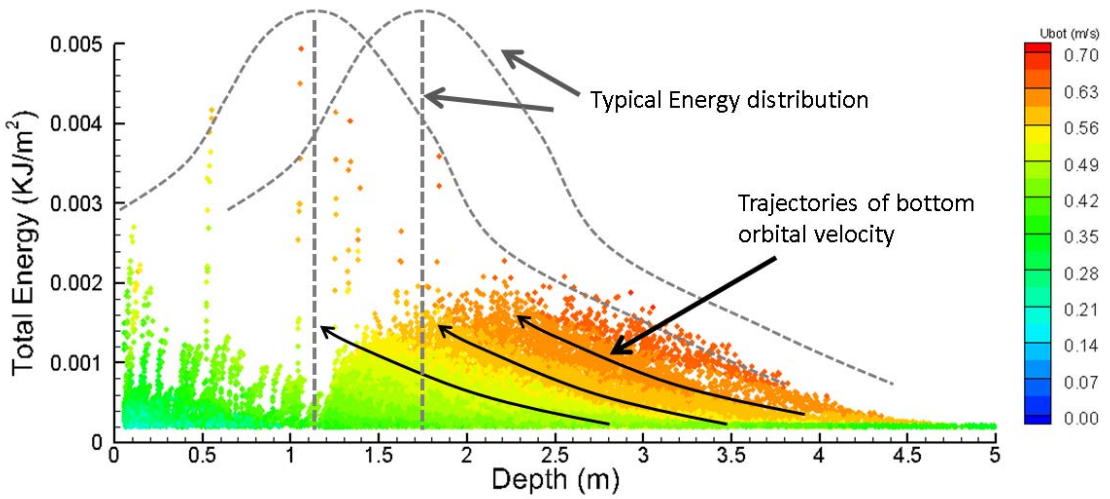

Figure 2 Typical distribution of energy dissipation versus depth. Filled circles also show the intensity of the wave bottom orbidal velocity (m/s) for the corresponding wave.

Orbital velocity increases with increasing wave height and therefore, bottom velocities are greater for large waves shoaling and breaking in deep water compared to smaller waves in shallow water. This condition is illustrated in Figure 2, as indicated by the isovels (lines of equal velocity - color bar, and trajectory arrows), which show that velocities decline rapidly as waves transition into shallow water.

Distribution of Energy dissipation

Wave energy dissipation for the four study sites is shown in Figure 3. The histograms indicate a clear peak in energy dissipation along the Terrebonne barriers (Figure 3, upper right) at the 1.5 m depth, followed by secondary peaks at around 1 and 2 m, respectively. This trend is similar along Pelican island and vicinity, where we see (Figure 3, upper left) a clear peak in frequency around 1.5 m and a second peak at about ~2 m. Conditions along the Chandeleur shoreline appear to behave differently, exhibiting a more uniform distribution of wave energy dissipation, which generally occurs in deeper water. Similarly, the Barataria shore demonstrates a more uniform energy dissipation with peaks at the 3 m isobaths. Comparatively, the Barataria shore receives approximately one half the frequency of energy dissipation of the other sites. This pattern suggests that energy is dissipated over a range of depths, as illustrated by the lack of a

peak in the histogram (Figure 3). One possible explanation for this phenomenon is that waves along the Chandeleurs enter shallower water without transforming significantly and then break in the surfzone. This behavior is supported by the decline in the frequency around 1.5 m, followed by an increase at depths of 1m or less. The overall flat nature of the nearshore and upper shore face slope likely contribute to this process.

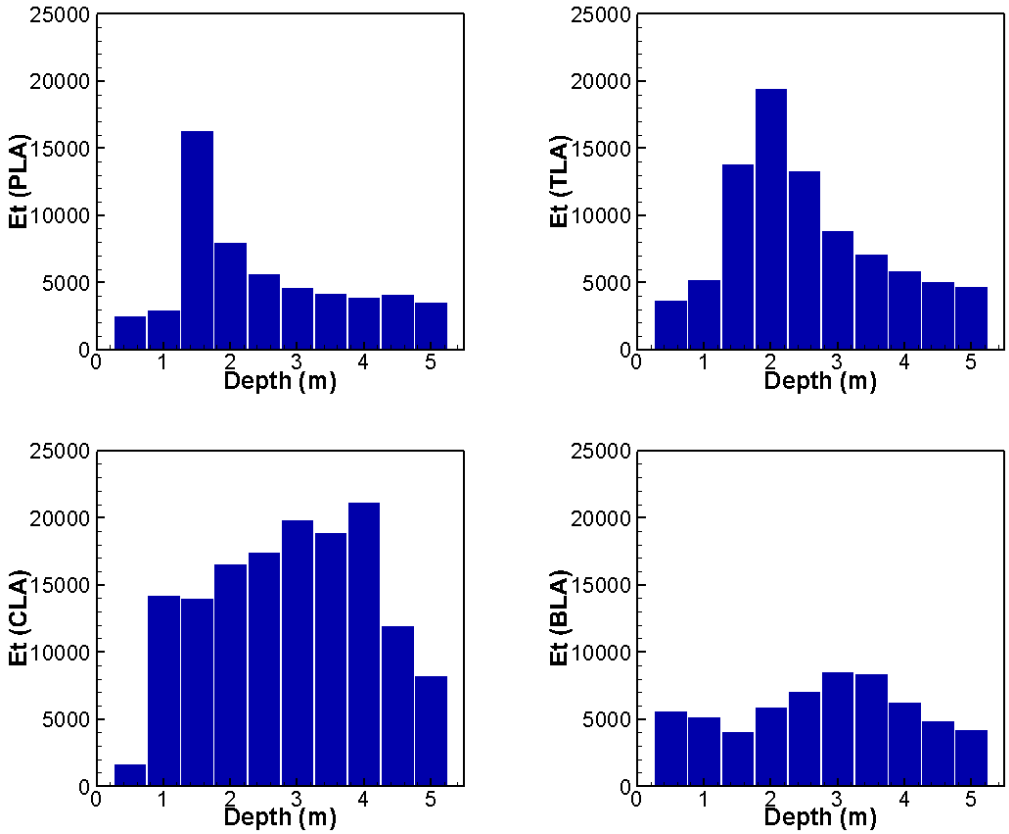

Figure 3 Histograms of total wave energy dissipation (white-capping plus surfzone) for each of the study sites plotted against depth. Note that the peak frequency occurs between 1 and 2 meters, except for the Chandeleurs and the Barataria, where the distribution appears somewhat uniform. Results include all scenarios simulated (40 scenarios – typical year). Locations for model domains are shown in Figure 1

Summary of simulations using all scenarios

The authors have used a previously developed SWAN model to assess the potential wave energy dissipation along study areas in Louisiana and Mississippi. Dissipation terms were computed by the model and outputted directly. This study used the sum of all dissipation terms to account for the energy lost due to dissipation, and carried out frequency analysis to determine the distribution of energy dissipation across selected depth increments. Generally, the model results show a large peak in the energy dissipation frequency, indicating a likely position of wave transformation and sand entrainment into the water column. This position was consistent at the Terrebonne and Pelican Island sites, with a peak frequency occurring at approximately 1 – 2 m. The Chandeleur Islands and Barataria shorelines showed a more uniform distribution compared to the Terrebonne and Pelican sites and higher and lower wave energy dissipation respectively. This pattern suggests that the underlying wave transformation processes are different at these sites. The uniform distribution at the Chandeleur Islands suggests that waves are transforming at a slower rate and are less likely to entrain sediment near the surface water, except within the surfzone. The lower energy dissipation simulated along the Barataria shoreline suggests that waves maintain their energy at depths of ~ 3 m, and transform rather slowly until they again reach the surfzone, generally at a depth of less than 2 m.

Energy dissipation analysis during time of oiling

Although Figure 3 shows results from all scenarios, it is important to assess the wave climate, and the energy dissipation during times when surface oil was present. Therefore, oiling information (segment location, period of oiling, type of oiling as recorded by shoreline cleanup assessment team [SCAT]) was obtained and plotted against wave modeling results. The corresponding wind speed, direction, and respective wave climate during oiling conditions were identified and used for further analysis. Once the oiling time interval was identified, the energy dissipation analysis was repeated for that time period (Figures 4 and 5).

Barataria (BLA) and Terrebonne (TLA) Shorelines

The Barataria shoreline model (BLA) covers the area from Belle Pass to East Grand Terre. Wave energy dissipation at the time of oiling is shown in Figure 4 (top left and right). Figure

4 (top right) shows the histogram of energy dissipation occurring as a function of depth and Figure 4 (top left) shows the specific energy dissipation peak calculated within each of the depth bins as indicated in Figure 4 (top right). For example, although there appears to be a gradual decay of energy from depth 2 – 5 m (Figure 4 top right), the specific energy dissipation appears to be reaching maxima around a depth of 0.5 m. Additional energy dissipation takes place between 0.5 and 2 m and beyond the 2 m isobath, energy dissipation appears to decay exponentially. A sensitivity analysis performed by adjusting the initial water level for each simulation to represent high and low tide conditions, yielded no significant differences. For example, the histogram shape appears to be the same, except that at low tide the 0.5 m isobaths would be shifted offshore and during high tide the same effect would shift the 0.5 m isobath landward where energy is dissipated.

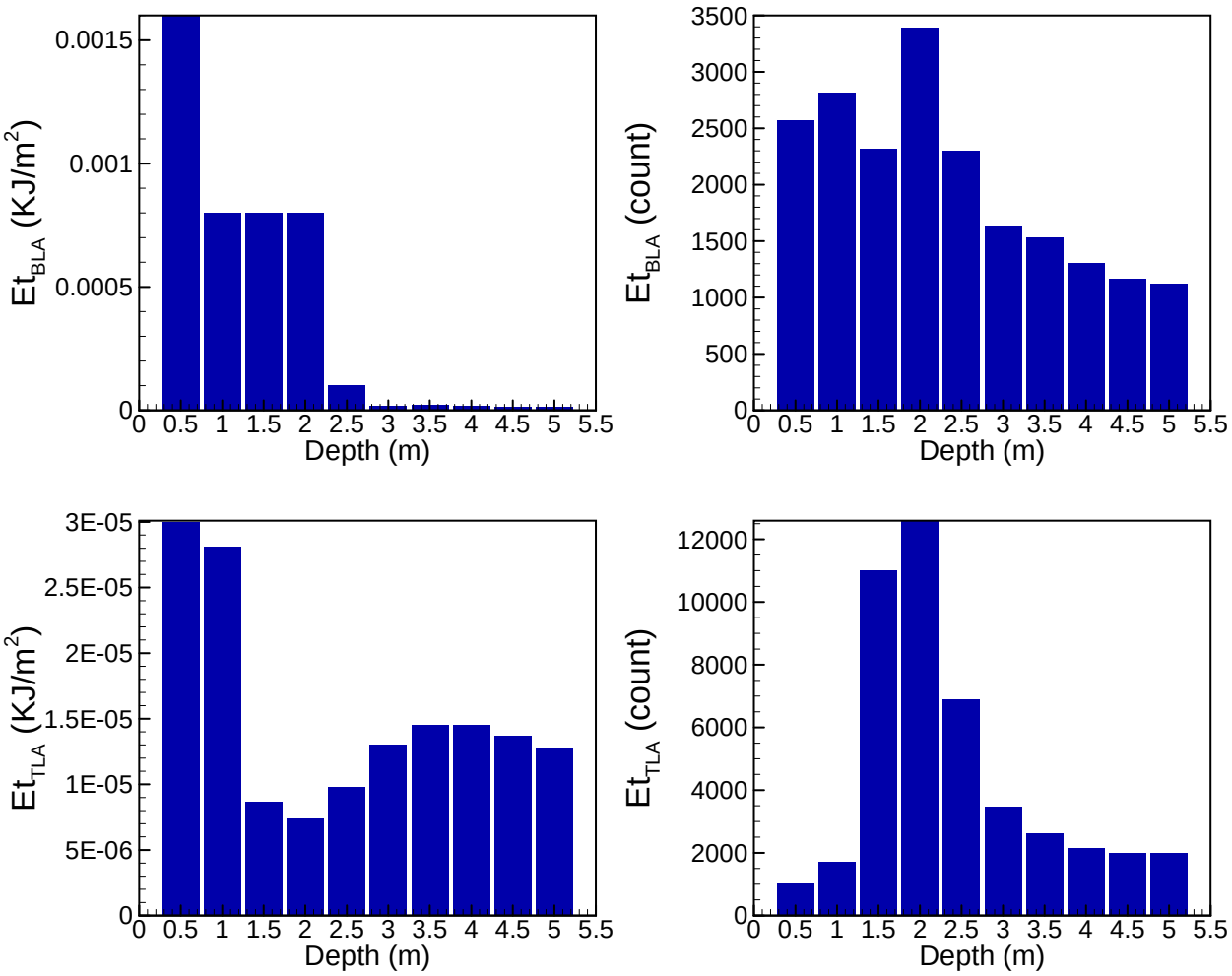

Figure 4 Histograms of total wave energy dissipation (whitecapping plus surfzone) and total energy frequency (count) for BLA (Barataria shoreline segment - top) and TLA (Terrebonne shoreline segment - bottom) plotted against depth. Note that the peak frequency occurs between 0.5 and 2 meters. This analysis includes only waves that occurred during oiling conditions at these locations based on SCAT reports.

Pelican and Chaland (PLA) shorelines and Chandeleur Islands (CLA)

The model domain covering the east Barataria shorelines includes Pelican and Chaland Islands and adjacent shorelines. A final model domain covers the Chandeleur Islands. The wind and wave climate during time of oiling were used as representative conditions for wave simulations and analysis. Figure 5 (top right) shows the histogram of energy dissipation versus depth for the Pelican-Chaland shoreline, indicating a distinctive peak at a depth of 1.5 m. The specific energy dissipated at each of the depth bins shows a corresponding peak at a similar depth (1.5 - 2 m), suggesting that this is where most waves were breaking and dissipating most of their energy.

Similar to the Barataria and Terrebonne shorelines, beyond a depth of approximately 2 m, an exponential decay of energy dissipation occurs, suggesting further that the energy dissipated at those depths is relatively smaller (Figure 5 top).

The Chandeleur Islands (CLA) exhibit a somewhat different condition. For instance, although the histogram of energy dissipation frequency (count) shows that there is a uniform pattern in energy dissipation peaking between depths of 1.5 – 3 m, the corresponding peak in the mean energy within each of the depth bins peaks at a depth of approximately 1 m, with a significant decline of the mean energy dissipation deeper than this depth. This suggests that the likely position of the energy dissipation maxima occurs at a depth of approximately 1 m.

Mississippi Barrier Shorelines

The model domain for the Mississippi Barriers covers all the barriers and is shown in Figure 1. The total energy distribution (Figure 5 left) shows peaks at 1.5, 2.5, and 4 meters of water in terms of occurrence, however, the specific energy dissipated (Figure 5, right) shows a distinctive peak around 1 m, ranging from 0.5 – 1.5 m, suggesting that most energy is dissipated insight the 2 m isobaths, which is consistent with other sites in Louisiana.

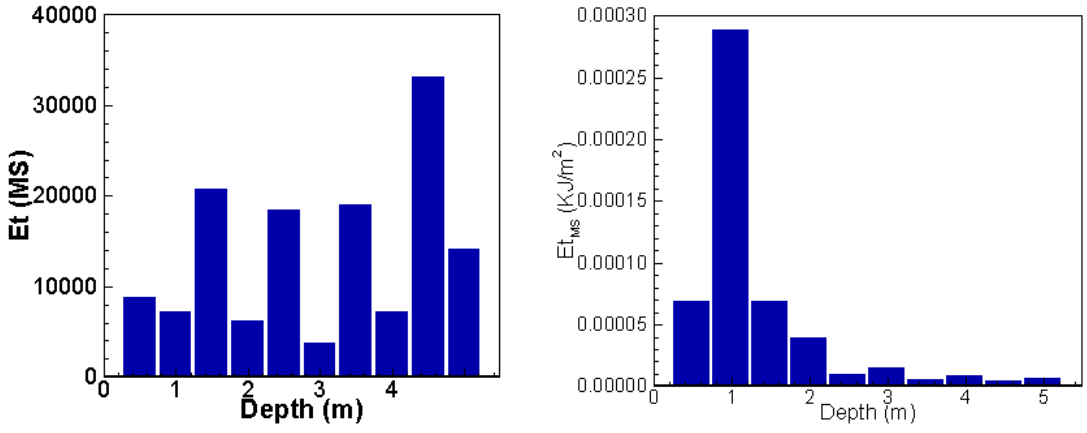

Figure 5 Histograms of total wave energy dissipation (whitecapping plus surfzone) and total energy frequency (count) for Mississippi State barrier Islands (MS) plotted against depth. Note that the peak frequency occurs between 0.5 and 1.5 meters. This analysis includes only waves that occurred during oiling conditions at these locations based on SCAT reports.

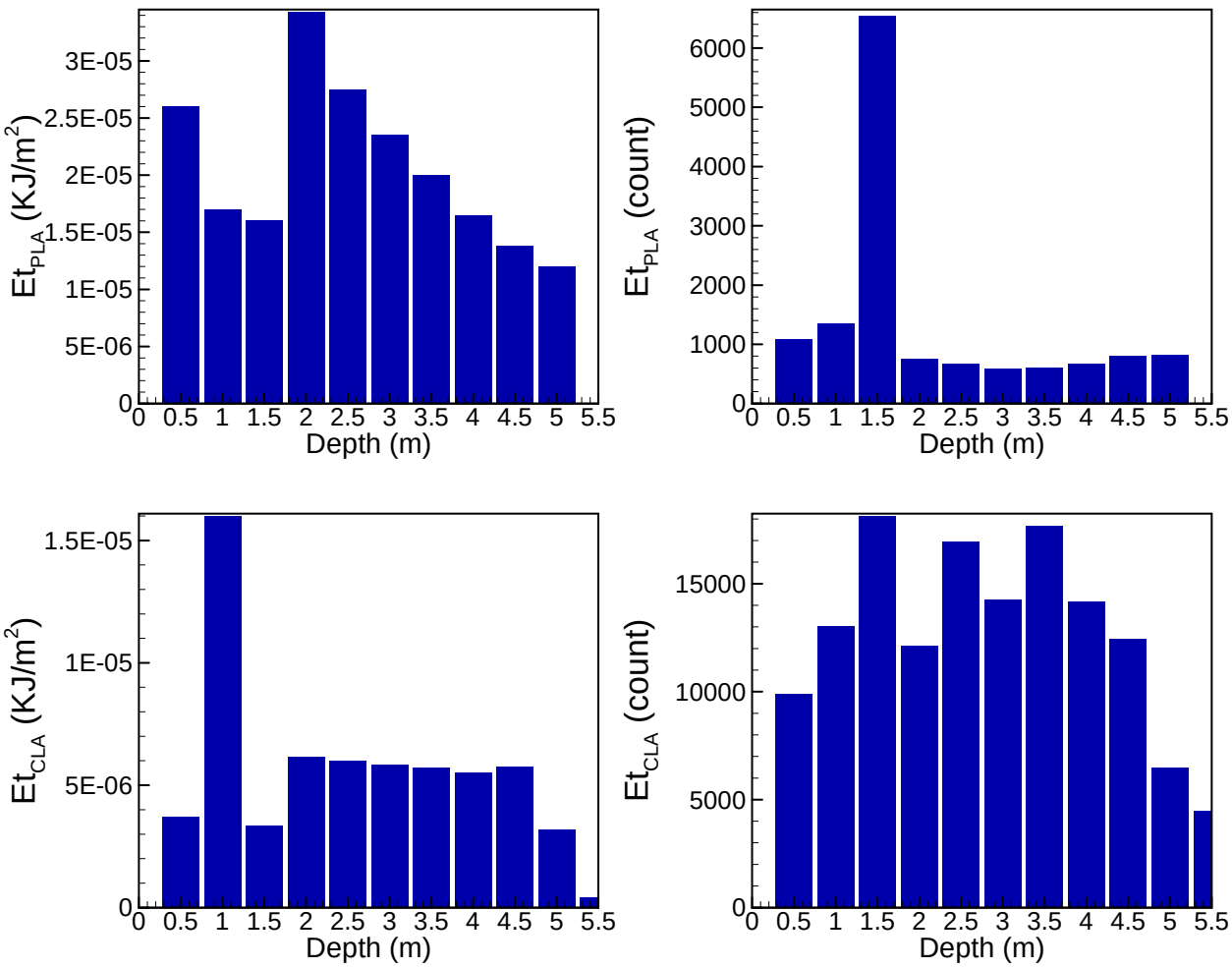

Figure 6 Histograms of total wave energy dissipation (whitecapping plus surfzone) and total energy frequency (count) for PLA (Pelican Island segment - top) and CLA (Chandeleur Islands segment - bottom) plotted against depth. Note that the peak frequency occurs between 0.5 and 2 meters. This analysis includes only waves that occurred during oiling conditions at these locations based on SCAT reports.

Entrainment of marine sands

The shear produced by breaking waves can often introduce sand in suspension (Soulsby, 1997). Although most of the sand remains within the wave boundary layer, which is relatively small, the actual depth or height above the bed where sand can be entrained is a function of many variables (Nielsen, 1992), including, wave characteristics (e.g. period, bottom orbital velocity), bed friction (ripples, flat beds, other), and median grain diameter and settling velocity. Nielsen (1992) derived a set of equations that treat the suspended concentrations under waves and waves with currents. Once suspended, sand will occupy the water column above the bed with a

theoretical profile that decays exponentially, similar to a Rouse profile (Rouse, 1949). The concentration above the bed is then given by

$$C_{(z)} = C_0 e^{-\frac{z}{l}}$$

where C_0 is the reference concentration near the bed and *l* is the decay length scale. Following Nielsen (1992):

$$l = 0.075 \frac{u_b}{w_s} \Delta_r \qquad \text{for} \qquad \frac{u_b}{w_s} < 18$$

$$l = 1.4 \Delta_r \qquad \text{for} \qquad \frac{u_b}{w_s} \geq 18$$

$$C_0 = 0.005 \Theta_r^3$$

where

$$\Theta_r = \frac{f_{wr} u_b^2}{2(s-1) g D \left(1 - \frac{\pi \Delta_r}{\lambda_r}\right)^2}$$

$$f_{wr} = 0.00251 \exp(5.21 r^{-0.19})$$

$$r = \frac{u_b T}{5 \pi D_{50}}$$

are, respectively, the critical entrainment function Θ_r, the friction factor f_{wr}, Δ_r is the ripple height, λ_r is the ripple length, u_b is the bottom orbital velocity and T is the wave period. Analysis using the Nielsen (1992) equations based on wave information during oiling conditions suggests that the energy dissipated is too small to entrain sand up to the surface of the water column. Thus, although sand is very likely in suspension, our analysis shows that surface concentrations would be extremely low. The range in height above the bed for sand suspension varies from centimeters to slightly above 0.5 m, given wave conditions provided by the model

during oiling for each of the locations. Although there is some uncertainty associated with the analysis, generally at the corresponding depths where peak energy dissipation occurs, it is very unlikely that suspended sand could reach the surface of the water column. This suggests a different mechanism for mat formation in Louisiana, such as the creation of a sand and oil slurry in the swash zone by wave swash and backwash along the beachface. As more sand is added to this agglomeration, a mat forms and stabilizes in the intertidal or subtidal zone. Secondly, floating oil washed ashore and became stranded by the falling tide. In the warm sun the oil seeped into the sand and stabilized in the upper to lower intertidal zone.

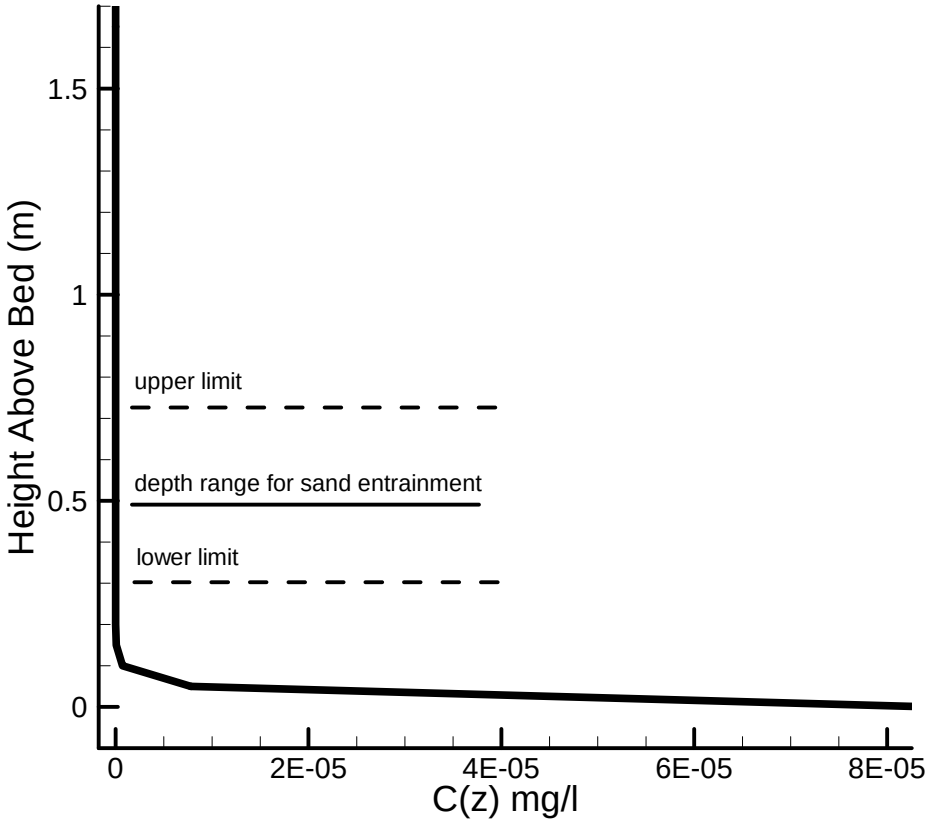

Figure 7 Typical profile of sand entrainment above the bed for wave conditions during oiling in Louisiana. The range of depths where we notice sand in suspension varies from centimeters to slightly above 0.5 m, given wave conditions provided by the model. Uncertainty in the analysis is present, but generally at the corresponding depths where energy is dissipated it is not likely that sand reaches the surface of the water column.

References

Booij, N., Ris, R.C., and Holthuijsen, L.H., 1999, A third-generation wave model for coastal regions—1. Model description and validation: Journal of Geophysical Research, v. 104, no. C4, p. 7649–7666.

Soulsby, R.L., 1997, Dynamics of marine sands—A manual for practical applications: London, Thomas Telford Publications, 249 p.

Soulsby, R.L., and Damgaard, J.S., 2005, Bedload sediment transport in coastal waters: Coastal Engineering, v. 52, no. 8, August, p. 673–689.

Georgiou, I.Y., Hughes, Z.J., Trosclair, K., 2013. Application of Hydrodynamic and Sediment Transport Models for Cleanup Efforts Related to the Deepwater Horizon Oil Spill Along the Coast of Mississippi and Louisiana, Technical Report prepared for OSAT3, 44pp.

Nielsen, P., 1992. Costal bottome boundary layers and sediment transport, Advanced Series in Ocean Engineering, Volume 4, World Scientific, New Jersey, USA,324 pp.

Rouse, H., 1949. Engineering Hydraulics, Ed. Hunter Rouse, John Wiley and Sons, New York, USA, 1039pp.